DOI: 10.1002/ejic.200500835

pH-Specific Synthesis and Structural and Spectroscopic Characterization of a Complex between Co^{II} and *N*,*N*-Bis(phosphonomethyl)glycine: Cobalt–Phosphonate Interactions in the Solid State and in Solution

Anca Mateescu,[a] Catherine P. Raptopoulou,[b] Aris Terzis,[b] Vassilis Tangoulis,[c] and Athanasios Salifoglou*[d]

Keywords: Cobalt / Magnetic properties / Materials science / Phosphonates / Structural speciation

The presence of cobalt in biological systems has been associated with a variety of regulatory roles as an inorganic cofactor. Its involvement in (bio)chemical processes, where it contributes to the integrity of the physiology of humans, underscores its ability to promote (bio)chemistry with molecular targets of variable mass and biological properties. Given the fact that organic phosphonates are widespread substrates/ligands in biological fluids, we sought to investigate the relevant chemistry with Co^{II}. With the organophosphonate ligand *N*,*N*-bis(phosphonomethyl)glycine (H_5NTA2P) as the main metal ion binder, aqueous reactions with Co^{II} were examined, ultimately leading to the isolation of the complex $[Co(C_4H_9O_8NP_2)(H_2O)_2]\cdot 2H_2O$ (**1**) at pH 1.5. This complex was characterized analytically, spectroscopically (FT-IR, UV/Vis, EPR), magnetically, and by cyclic voltammetry. X-ray crystallography shows that **1** is a compound with a molecular type of lattice. The complex consists of a mononuclear, octahedral Co^{II} center coordinated by oxygen atoms belonging to the terminal phosphonate and carboxylate groups of H_3NTA2P^{2-}, the ligand nitrogen, and two bound water molecules. It should be emphasized that similar structural features have been observed in other metal organophosphonate lattices of materials with potential catalytic and chemical reactivity. The magnetic and EPR data for **1** suggest the presence of a high-spin octahedral Co^{II}, with a ground state of an effective spin $S = 1/2$. The solution UV/Vis and EPR spectra suggest retention of the integrity of **1**, which is consistent with the magnetization measurements in the solid state. Collectively, the data suggest a soluble Co^{II}–organodiphosphonate species, not unlike those expected in bio-fluids containing the specific ligand or ligands structurally akin to H_3NTA2P^{2-}.The biological relevance of **1** to species in biofluids and the structural association with Co^{II}–organophosphonate materials is discussed.

Introduction

Cobalt has been known to be present in biological systems for a long time. Its involvement in biomolecular activity is intimately linked to its entry in molecular targets like B_{12} coenzyme and vitamin B_{12} and its potential as an inorganic cofactor to influence biological processes.[1–4] To this end, cobalt has been found in metallohydrolases like methionine aminopeptidase,[5] nitrile hydratases,[6] ribonucleotide reductase, glutamate mutase, and others.[7] Beyond that, an absence or excess of cobalt has been linked to pathological aberrations in human physiology. In particular, vitamin B12 deficiency has been linked to pernicious anemia,[8] while overexposure to the metal has been associated with toxic effects linked to heart disease and excessive formation of red corpuscles.[9,10]

Understanding the role of cobalt in those biological systems entails a deep understanding of its (bio)chemical interactions with low as well as high molecular mass biomolecules in the requisite fluids.[2,3,6,7] These interactions reflect the potential binding of cobalt to organic substrates/ligands of variable structure and function in physiological or aberrant processes thereof. The binary and ternary species of cobalt thus formed participate in complex equilibria, the delineation of which is essential in defining soluble bioavailable species that actively participate in bioprocesses. At the low mass end of the spectrum of molecular targets are molecules like organic acids, amino acids, small peptides, and other molecules that possess variable structural features, prominent among which are the carboxylate and phosphonate groups.[11] Phosphonate groups are known to participate in key phosphorylation events that influence the (bio)chemical activity, signal transduction, enzyme inhibition, neuroactivity, plant-growth regulation, antibiotic, and herbicidal activity of both small and large molecules.[11,12]

[a] Department of Chemistry, University of Crete, Heraklion 71409, Greece
[b] Institute of Materials Science, NCSR "Demokritos", Aghia Paraskevi 15310, Attiki, Greece
[c] Department of Materials Science, University of Patras, Patras 26500, Greece
[d] Laboratory of Inorganic Chemistry, Department of Chemical Engineering, Aristotle University of Thessaloniki, Thessaloniki 54124 and Chemical Process Engineering Research Institute, Thermi, Thessaloniki 57001, Greece
Fax: +30-2310-996-196
E-mail: salif@auth.gr

Organophosphonates are a particularly interesting family of organic targets in the biochemistry of metal ions and the chemistry of materials.[13] Such materials have been known for some time for their versatility in coordination and variability in nuclearity.[14] Both these properties are intimately associated with variable dimensionality[15] materials and layered metal organophosphonates[16] and also with a diverse reactivity that is linked to catalysis, intercalation chemistry, optical properties of novel materials, and others.[17,18]

The significance of metal organophosphonate chemistry in the fields of research mentioned above necessitates the extensive perusal of the relevant chemistry with Co^{II}, many aspects of which[19] have yet to be discovered. Bearing in mind that the structural features of potential metal ion binders, like organophosphonates, dictate the chemistry of interactions with the metal ion under investigation and most likely influence any arising physical and/or biological properties, we have launched research efforts targeting the reactivity of one such class of diphosphonic ligands toward Co^{II}. Herein, we report on the synthesis, isolation, spectroscopic and structural characterization, and cyclic voltammetric, magnetic, and EPR studies of a new species between Co^{II} and the carboxydiphosphonate ligand *N*,*N*-bis(phosphonomethyl)glycine (H_5NTA2P).

Results and Discussion

Synthesis

The synthesis of complex **1** was carried out in aqueous solutions containing Co^{II} and *N*,*N*-bis(phosphonomethyl)-glycine. The overall reaction leading to compound **1** is depicted schematically below.

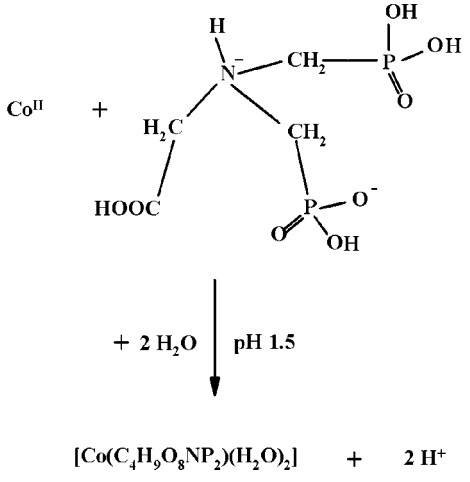

The metal-to-ligand stoichiometry employed was 1:1, with a pH of 1.5. Slow diffusion of ethanol into the reaction mixture led to the precipitation of well-formed pink prismatic crystals. Elemental analysis of the crystalline material was consistent with the formulation $[Co(C_4H_9O_8NP_2)(H_2O)_2]\cdot 2H_2O$ for complex **1**. The yield of the reaction was approximately 60%.

The isolated crystalline material **1** appears to be stable in the solid state for long periods of time, with no discernible deterioration. Complex **1** is soluble in water and insoluble in alcohols (CH_3OH, *i*PrOH), acetonitrile, and DMSO.

X-ray Crystal Structure of $[Co(C_4H_9O_8NP_2)(H_2O)_2]\cdot 2H_2O$ (1)

The X-ray crystal structure of **1** reveals the presence of a molecular lattice. The compound crystallizes in the monoclinic system $P2_1$. Crystallographic details are given in the Experimental Section. The ORTEP diagram of **1** is shown in Figure 1, and selected interatomic distances and bond angles for **1** are listed in Table 1. The structure consists of a mononuclear core unit containing an octahedral Co^{II} ion. The coordination sphere of Co^{II} is formulated by an oxygen–nitrogen donor atom environment created by the two main participant ligands, namely bis(phosphonomethyl)glycinate [$(^{-}HO_3PCH_2)_2NCH_2COOH$ = H_3NTA2P^{2-}] and water. More specifically, each H_3NTA2P^{2-} ligand, employing both phosphonate groups as well as the carboxylic terminal oxygen, coordinates to the metal ion through its singly deprotonated phosphonates, with the carboxylic acid anchor staying in its protonated form. In addition, two water molecules are coordinated to the Co^{II} ion. Both they as well as the H_3NTA2P^{2-} ligand fulfill the coordination requirements of the octahedral sphere around Co^{II}. A closer look at the octahedron shows that one of the water molecules along with the two phosphonate oxygens and the terminal carboxylate of the H_3NTA2P^{2-} ligand form the equatorial plane of the octahedral metal ion. The second bound water molecule along with the nitrogen of the H_3NTA2P^{2-} ligand bound to Co^{II} occupy the axial positions in the octahedron. In view of the above description and the available structural data, the mononuclear Co^{II} ion resides in a distorted octahedron.

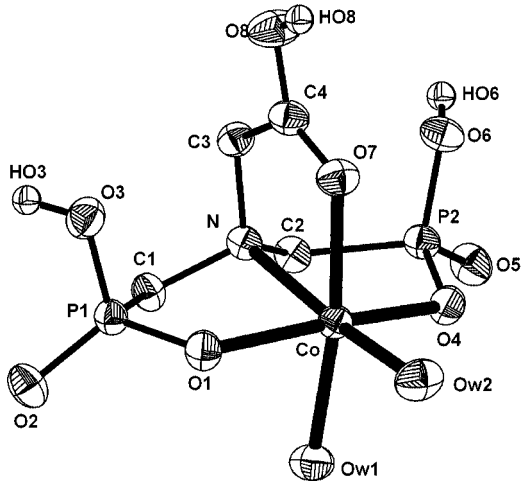

Figure 1. The molecular structure of the $Co(C_4H_9O_8NP_2)(H_2O)_2$ unit, with the atom labeling scheme in **1**. Thermal ellipsoids represent 50% probability surfaces.

The Co–O distances in **1** are similar to those observed in other mononuclear octahedral Co^{II} sites, among which are

Table 1. Bond lengths [Å] and angles [°] for $[Co(C_4H_9O_8NP_2)(H_2O)_2]\cdot 2H_2O$ (**1**).

Co–Ow2	2.012(2)	Co–Ow1	2.127(2)
Co–O(1)	2.100(2)	Co–O(7)	2.141(2)
Co–O(4)	2.101(2)	Co–N	2.229(2)
Ow2–Co–O(1)	95.99(8)	O(4)–Co–O(7)	97.58(8)
Ow2–Co–O(4)	95.41(9)	Ow1–Co–O(7)	172.24(8)
O(1)–Co–O(4)	164.81(7)	Ow2–Co–N	173.94(9)
Ow2–Co–Ow1	90.06(9)	O(1)–Co–N	84.22(7)
O(1)–Co–Ow1	82.68(8)	O(4)–Co–N	85.51(7)
O(4)–Co–Ow1	87.30(8)	Ow1–Co–N	95.97(8)
Ow2–Co–O(7)	95.46(9)	O(7)–Co–N	78.47(7)
O(1)–Co–O(7)	91.30(8)		

those in $[Co(C_2H_8O_6NP_2)_2(H_2O)_2]$ [2.067(2)–2.132(2) Å] (**2**),[20] $(NH_4)_4[Co(C_6H_5O_7)_2]$ [2.051(2)–2.157(2) Å] (**3**),[21] $[Co\{COOCH_2CH(OH)COO\}]\cdot 3H_2O$ [2.067(3)–2.136(3) Å] (**4**),[22] the phosphonate derivatives $[Co(NH_3CH_2PO_3)_2(H_2O)_2]_n\cdot nH_2O$ [2.104(4)–2.121(4) Å] (**5**),[23] $[Co\{HO_3PC(CH_3)(OH)PO_3H\}_2(H_2O)_2][NH_2(C_2H_5)_2]_2$ [2.064(2)–2.179(2) Å] (**6**),[24] and $[Co(OPMe_3)_3(H_2O)_2]I_2\cdot[Co(OPMe_3)_3(H_2O)_3]I_2$ [1.87(6)–2.18(4) Å for the octahedral site].[25]

The Co–O distances in the equatorial plane of the octahedron are of similar length [2.100(2)–2.141(2) Å], despite the variable nature of the anchor terminals in the two different ligand components in the coordination sphere of Co^{II} and the fact that they all utilize their oxygens as terminal anchors to the metal ion. In contrast to the equatorial distances, the corresponding axial Co–L bonds reflect more radically varying lengths, with the Co–N distance being about 0.1 Å longer than the equatorial ones, while the Co–O_w distance is about 0.1 Å shorter than the equatorial ones. It is not unlikely that such bond-length variations might be due to Jahn–Teller distortions, which are usually encountered in high-spin Co^{II} octahedral species.

The angles within the equatorial plane defined by O(1), O(4), $O_w(1)$, and O(7) are in the range 82.68(8)–97.58(8)°, with the average being very close to the ideal octahedral angle of 90°. A similar yet wider angle variation is observed between the axial donor atoms N and $O_w(2)$ and those in the equatorial plane [range: 78.47(7)–95.99(8)°]. The aforementioned sets of angles are similar to those observed in **2**–**6** and in the complexes $[Cu\{HO_3PC(CH_3)(OH)PO_3H\}_2(H_2O)_2]^{2-}$ [84.7(2)–95.3(2)° and 87.8(2)–92.2(2)°, respectively][24] and $[Zn\{HO_3PC(CH_3)(OH)PO_3H\}_2(H_2O)_2]^{2-}$ [84.98(6)–95.02(6)° and 88.65(6)–91.37(6)°, respectively].[26]

The H_3NTA2P^{2-} ligand in **1** binds to the central metal ion through all of its available anchors each in a unidentate coordination mode. This is in contrast to the bidentate mode of coordination that the H_3IDA2P^- ligand employs in its binding to the same metal ion in $[Co(C_2H_8O_6NP_2)_2(H_2O)_2]$. The latter observation is exemplified through the binding of the two phosphonate anchors to two different Co^{II} ions. Moreover, the four H_3IDA2P^- molecules surrounding the central metal ion are also coordinated to four other Co^{II} ions as a consequence of the presence of the second phosphonate group in each molecule. In this sense, occupancy of the coordination sites in contiguous octahedral Co^{II} ions extends to infinity, thus affording the molecular lattice in **2**.

Another interesting attribute of the H_3NTA2P^{2-} ligand's participation in the coordination sphere of Co^{II} is the presence of a nonprotonated central imino moiety in the ligand.

Table 2. Hydrogen bonds in $[Co(C_4H_9O_8NP_2)(H_2O)_2]\cdot 2H_2O$ (**1**).

Interaction	D···A [Å]	H···A [Å]	D–H···A [°]	Symmetry operation
O3–HO3···O5	2.547	1.704	174.9	1 – *x*, –0.5 + *y*, 1 – *z*
O6–HO6···O1	2.559	1.812	174.2	1 + *x*, *y*, *z*
O8–HO8···O4	2.593	1.850	158.7	1 – *x*, –0.5 + *y*, –*z*
Ow1–Hw1A···Ow3	2.720	1.841	166.4	*x*, *y*, *z*
Ow1–Hw1B···O5	2.922	2.111	166.7	–1 + *x*, *y*, *z*
Ow2–Hw2A···Ow4	2.672	1.906	162.6	–*x*, 0.5 + *y*,–*z*
Ow2–Hw2B···O2	2.691	1.845	167.8	*x*, *y*, –1 + *z*
Ow3–Hw3A···O2	2.785	1.970	166.8	–*x*, 0.5 + *y*, 1 – *z*
Ow3–Hw3B···O6	2.934	2.187	157.8	1 – *x*, 0.5 + *y*, –*z*
Ow4–Hw4A···O3	2.983	2.203	171.8	*x*, *y*, *z*

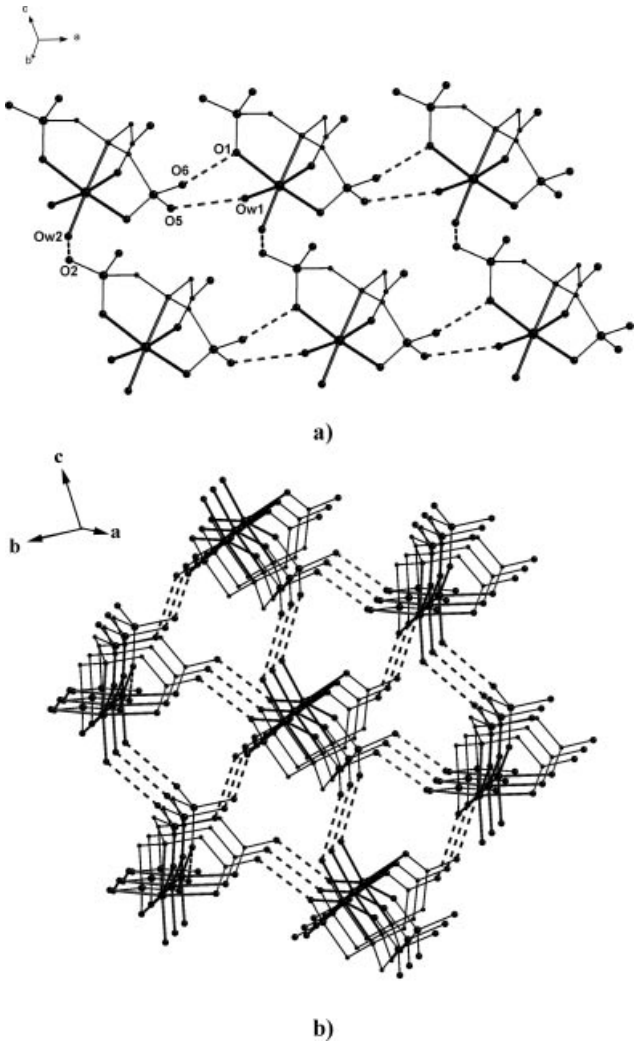

Figure 2. a) The polymeric chains of **1** along the *a* axis and their connection along the *c* axis due to hydrogen-bonding interactions (dashed lines). b) The 3D network of **1** formed by H bonds as shown looking down the *a* axis.

As a result, the overall charge of the H_3NTA2P^{2-} ligand coordinated to Co^{II} is 2–, which means that the overall charge for complex **1** is zero. Again, this behavior contrasts with that which has been previously observed for H_3IDA2P^- bound to Co^{II} in complex **2**. There, the central imino moiety of the bound ligand is protonated, thus yielding an overall charge of 1– for the ligand and a zero charge for the complex.

Hydrogen-bonding interactions are present in the crystal structure of **1** (Table 2). These interactions involve the coordinated water molecules, the phosphonate oxygen and hydroxy moieties on the H_3NTA2P^{2-} ligand, and the solvent water molecules. These hydrogen-bonding interactions (Figures 2, parts a and b) generate an extensive network, which very likely contributes to the overall stability of the crystal lattice in **1** (see Discussion).

Electronic Spectroscopy

The UV/Vis spectrum of **1** was recorded in water at the autogenous pH (Figure 3). The spectrum shows a shoulder-like band at around λ_{max} = 550 nm ($\varepsilon \approx 6.8$), ultimately reaching a well-formed major peak at λ_{max} = 517 nm (10), with ensuing, subtly discernible, shoulders at around 473 (4) and 462 nm (7.6). A distant band rising into the UV region appears at 222 nm (122.7). The absorption features are likely due to d–d transitions, which are typical for a Co^{II} d^7 octahedral species.[27] The multiply structured band around 517 nm can be tentatively attributed to the $^4T_{1g} \rightarrow {}^4T_{1g}(P)$ transition. The observed multiple structure is in line with literature reports that invoke an admixture of spin-forbidden transitions to doublet states derived from ^2G and ^2H, spin-orbit coupling, and vibrational or low-symmetry components to account for the complexity of the spectrum.[28] No further assignments can be made in the absence of detailed specific studies. The spectrum of **1** in water is different from that of Co^{II}_{aq},[29] thus indicating that the coordination sphere of Co^{II} in **1** is likely to be retained in solution.

FT-IR Spectroscopy

The FT-IR spectrum of complex **1** in KBr shows strong absorptions for the various vibrationally active groups. Antisymmetric as well as symmetric vibrations for the carboxylate group of the coordinated H_3NTA2P^{2-} ligand dominate the spectrum. Specifically, the antisymmetric stretching vibrations, $\nu_{as}(COO^-)$, are present for the carboxylate carbonyls at around 1664 cm^{-1}, with the symmetric vibrations, $\nu_s(COO^-)$, for the same group appearing in the range 1461–1408 cm^{-1}. The frequencies of the observed carbonyl vibrations are shifted to lower values in comparison to the corresponding vibrations in the free H_5NTA2P acid. The difference between the symmetric and antisymmetric stretches, $\Delta[\nu_{as}(COO^-) - \nu_s(COO^-)]$, is greater than 200 cm^{-1}, which indicates that the carboxylate group of the H_3NTA2P^{2-} ligand is either free or coordinated to the metal ion in a monodentate fashion.[30] This was further confirmed by the X-ray crystal structure of **1**.

Vibrations for the PO_3 groups were observed for the antisymmetric stretching vibrations, $\nu_{as}(PO_3)$, between 1060 and 986 cm^{-1}. Symmetric stretching vibrations, $\nu_s(PO_3)$, were observed in the range 967–906 cm^{-1}. The frequencies for the aforementioned stretches appear to be shifted to lower values compared to those of free H_5NTA2P acid, thereby indicating changes in the vibrational status of the ligand upon binding to the Co^{II} ion.[31,32] The aforementioned tentative assignments are also in line with previous data reported for iminophosphonate-containing complexes of various metals.[33]

Cyclic Voltammetry

The cyclic voltammetric behavior of complex **1** was studied in aqueous solution at the autogenous pH, in the presence of KNO_3 as a supporting electrolyte. The cyclic voltammogram shows an irreversible oxidation wave at $E_{1/2}$ = 1.18 V vs. Ag/AgCl, corresponding to the Co^{II}/Co^{III} redox couple and a quasi-reversible wave (ΔE = 105 mV,

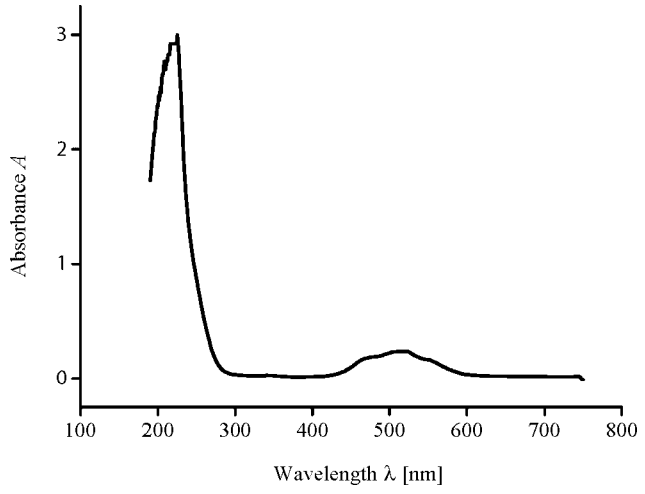

Figure 3. UV/Visible spectrum of **1** in water.

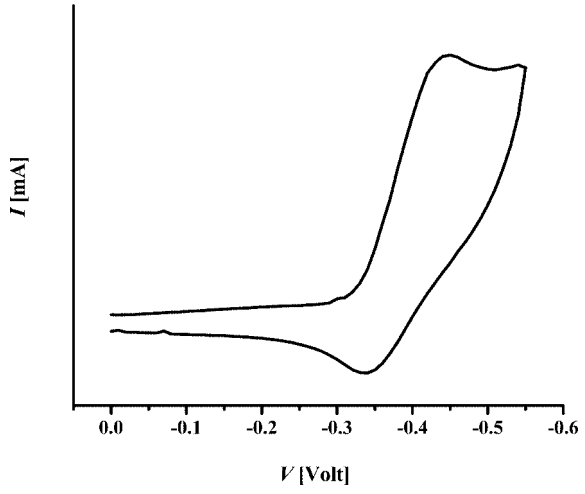

Figure 4. Cyclic voltammogram of **1** in water.

$0 < i_{pa}/i_{pc} < 1$, $i_{pc}/\{(v)^{1/2}C\}$ variable) at $E_{1/2}$ = –0.40 V vs. Ag/AgCl corresponding to the Co^{II}/Co^{I} redox couple (Figure 4). The observed $E_{1/2}$ value for the reduction wave is comparable to, albeit lower than, the one reported for other Co^{II}–organophosphonate species. Attempts to pursue the isolation of the one-electron-reduced product of the title complex **1** are currently ongoing.

Magnetic-Susceptibility Studies

Magnetic Susceptibility

Magnetic-susceptibility measurements were carried out at different magnetic fields and in the temperature range 2.3–300 K. Figure 5 shows the $\chi_M T$ vs. T susceptibility data at 0.1 T, where the solid line represents the fit according to the following general Hamiltonian [Equation (1)]

$$H = D\left[S_z^2 - \frac{1}{3}S(S+1)\right] + E(S_x^2 - S_y^2) + g\mu_B H \cdot S \quad (1)$$

where all the parameters have their usual definitions, and S = 3/2.

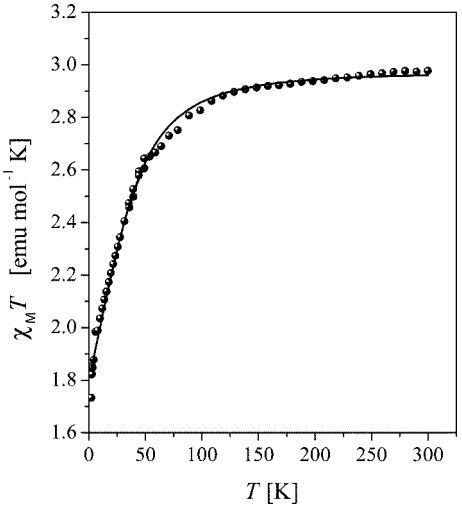

Figure 5. Temperature dependence of the magnetic susceptibility of **1**, in the form of $\chi_M T$ [emu mol^{-1} K] vs. T [K], in the temperature range 2.3–300 K using an external magnetic field of 0.1 T. The solid line represents the fitting results (see text).

The $\chi_M T$ values decrease smoothly from 2.98 emu mol^{-1} K at 300 K to 2.82 emu mol^{-1} K at 98 K and then more steeply to a value of 1.73 emu mol^{-1} K at 2.3 K. The high-temperature value of $\chi_M T$ is higher than 1.875 emu mol^{-1} K, the value that would be expected for a Co^{II} system with S = 3/2. This behavior is consistent with the presence of a significant orbital contribution to the anisotropic nature of the Co^{II} system investigated. The fitting model employed for the susceptibility data is shown in Equation (1). The model takes into account both the axial and rhombic parts of the distortion of the crystal field (D, E), and an isotropic g value, with the fitting results yielding the following parameters: D = 41.1 cm^{-1} and g = 2.53. The theoretical curve is shown as a solid line in the same figure. It must be pointed out that the signs of D and E cannot be resolved from the magnetic measurements, while introduction of an axial symmetry to g ($g_\perp$, $g_\parallel$) leads to no improvement of the fit. The large value of D is in accordance with an octahedral Co^{II}, where the ground-state doublet is well-isolated from the excited ones.[34]

Magnetization Studies

The magnetization data for **1** in the form of an $M/N\mu_B$ vs. H plot are shown in Figure 6 for two different temperatures and in the field range 0–6 T. The dotted lines represent the theoretical magnetization curves for a system having a ground state with an effective spin, S, of 1/2 and an effective g value equal to 4.697. The ground state of the free high-spin Co^{II} ion in an octahedral environment is ^4F, but the orbital degeneracy is removed in an octahedral crystal field, yielding one ^4A and two ^4T levels, with the lowest-lying state being a $^4T_{1g}$. The degeneracy of the $^4T_{1g}$ level is removed through the action of axial and rhombic distortions of the crystal field as well as through spin-orbit coupling. The overall effect of low-symmetry crystal-field components and spin-orbit coupling produces six Kramers doublets and results in a doublet ground state. Since the same doublet energy level remains lowest in energy for all values of the applied field strength, and the energy difference between the two lowest lying doublets is relatively large with respect to the thermal energy present at low temperatures (<30 K), the Co^{II} system may be described as having a ground state with an effective spin of S = 1/2.

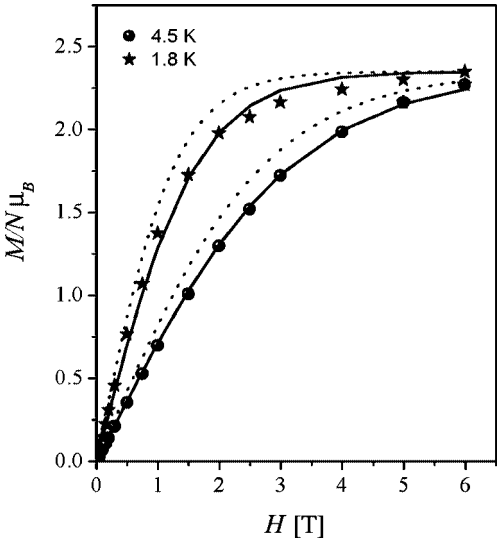

Figure 6. Magnetization of **1**, in the form of $M/N\mu_B$ vs. H [T], at different temperatures and in the field range 0-6 T. The dotted lines represent the theoretical Brillouin functions for an isolated S = 1/2 system with a g_{eff} = 4.697, while the solid lines represent a mean field correction (zJ = –1.5 cm^{-1}) taking into account the complex intermolecular interactions.

The discrepancy between the theoretical and the experimental curves is mainly due to the fact that a complex hydrogen-bonding network exists, which introduces intermolecular interactions that are important in the low-temperature regime.

A different magnetic model was used to fit the magnetization data according to the following modified Hamiltonian:

$$H = g\mu_B H \cdot S_z - zJ\langle S_z\rangle S_z \quad (2)$$

where the magnetic field is assumed to be along the z direction and the g-tensor is taken to be isotropic. $\langle S_z\rangle$ is given by the Boltzmann distribution law

$$\langle S_z\rangle = \frac{\sum_{M_s=-S}^{S} M_s \exp[-E(S,M_s)/kT]}{\sum_{M_s=-S}^{S} \exp[-E(S,M_s)/kT]} = \frac{\sum_{M_s=-S}^{S} M_s \exp\left[1 - M_s\left(g\mu_n H - zJ\langle S_z\rangle\right)/kT\right]}{\sum_{M_s=-S}^{S} \exp\left[1 - M_s\left(g\mu_n H - zJ\langle S_z\rangle\right)/kT\right]} \quad (3)$$

According to Equations (2) and (3) the magnetization formula becomes [Equation (4)]

$$M = -Ng\mu_B\langle S_z\rangle \quad (4)$$

with the negative sign originating from the negative charge of the electron.

An excellent agreement between the experimental modified and theoretical curves (solid lines) was obtained for the following fitting parameters: $zJ = -1.5$ cm^{-1}, $g_{eff} = 4.7$.

EPR Spectroscopy

X-Band EPR measurements were carried out in powder samples as well as in frozen solutions of **1** in water and are shown in Figures 7 and 8, respectively. As a consequence of the fast spin-lattice relaxation time of high-spin Co^{II}, signals were observed only below 70 K. For the powder spectra, a strong signal appears at low fields and a small broad one at $g = 2.30$ at temperatures below 23 K. In an attempt to comprehend the observed behavior, a simulation[34] was carried out in order to derive the effective g values riding on a Hamiltonian formalism [Equation (5)]

$$H = g_z\mu_B H_z S_z + g_x\mu_B H_x S_x + g_y\mu_B H_y S_y \quad (5)$$

with an effective spin of 1/2 and an anisotropic g-tensor. The results are shown in Figure 9. An isotropic magnetic-field domain line-width was used in both cases (lw = 35 G for the powder and 75 G for the frozen solution), with the broadness of the spectra revealing g-strain effects. Gaussian distributions of the g-principal values were used and the results were $\sigma g_x = \sigma g_z = 0.78$, $\sigma g_y = 0.23$ for the powder, and $\sigma g_x = \sigma g_y = \sigma g_z = 0.78$ for the frozen solution. The principal g values for the powder spectrum are $g_x = 4.92(1)$, $g_y = 2.28(1)$, $g_z = 6.33(1)$ ($g_{eff} = 4.51$) and for the frozen solution $g_x = 4.20(1)$, $g_y = 2.35(1)$, $g_z = 5.33(1)$ ($g_{eff} = 3.96$).

The dominant broadening effect emerges when the g-strain is converted into B-strain through the equation $\Delta B = -(h\nu/\mu_B)\cdot(\Delta g/g^2)$, where the parameters have their usual meaning. Thus, the largest and smallest g values of the powder and solution spectra have field widths that differ by an order of magnitude, thereby rationalizing the broad high-field features of the spectrum.

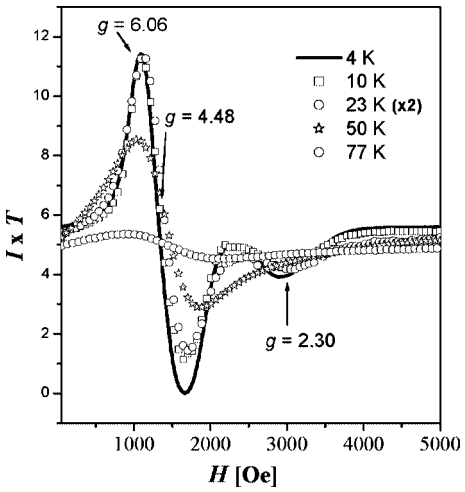

Figure 7. Temperature dependence of the powder X-Band EPR spectrum (the intensity is multiplied by the temperature) of **1** in the field range 0–5000 Oe.

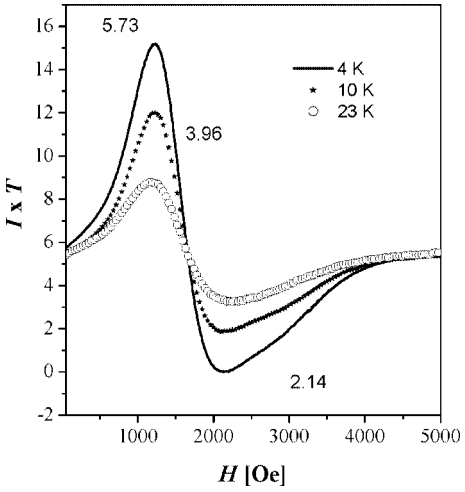

Figure 8. Temperature dependence of the water solution X-Band EPR spectrum (the intensity is multiplied by the temperature) in the field range 0–5000 Oe.

A very important feature of the Co^{II} ion is the value of the effective g parameter, g_{eff}, extracted from the EPR measurements, as a result of which interesting comments can be made. To this end, one important issue, not sufficiently discussed in the literature, pertains to an octahedron in a high-spin Co^{II} system with a small tetragonal or trigonal distortion, whereby additional terms are added in the ground-state doublet. Provided that these terms are small compared with the spin-orbit coupling of the ground-state doublet, they may be written in the form [Equation (6)]

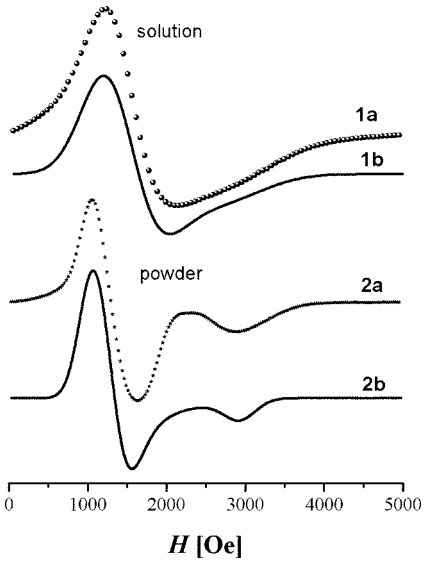

Figure 9. Simulations of the solution (1a) and powder (2a) EPR spectrum are shown as solid lines (1b) and (2b), respectively. The derived g values and the distribution widths of the g principal values in each case are given in the text.

$$\left|J=\frac{1}{2},J_z=\pm\frac{1}{2}\right\rangle+a\left|\frac{3}{2},\pm\frac{1}{2}\right\rangle+b\left|\frac{5}{2},\pm\frac{1}{2}\right\rangle \quad (6)$$

where a, and even more so b, are small compared to unity. According to Abragam and Bleaney,[35] and by neglecting terms of order a^2 and b^2, the expressions for the g parameters of the Co^{II} system are [Equations (7)]

$$g_{\parallel}=\frac{5}{3}g_s-\frac{2}{3}g_l+\left(\frac{4\sqrt{5}a}{3}\right)(2g_s-g_l)$$
$$g_{\perp}=\frac{5}{3}g_s-\frac{2}{3}g_l-\left(\frac{2\sqrt{5}a}{3}\right)(2g_s-g_l) \quad (7)$$

where $g_s = 2.0$ and $g_l = -3/2$.

The dependence of the g parameters on the a parameter of Equation (6) is shown in Figure 10. From Equations (7) and Figure 10, it is clear that the value of $g_{eff} = (g_{\parallel} + 2g_{\perp})/3 \approx (5g_s - 2g_l)/3 \approx 4.33$. Therefore, an isotropic g value of $g_{\parallel} = g_{\perp} = 4.33$ corresponds to $a = 0$ (the energy difference between the ground-state doublet and the excited one is very large), whereas for an admixture of other terms the value of g_{eff} increases accordingly (Figure 10).

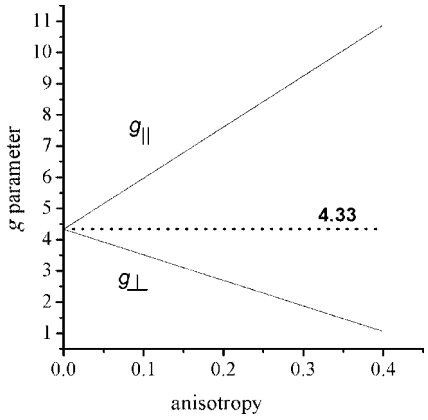

Figure 10. Anisotropy dependence of the g parameters ($g_{\parallel}$ and $g_{\perp}$) of a high-spin Co^{II} octahedron resulting from a small tetragonal or trigonal distortion.

Another issue emerges from the fact that weak intermolecular interactions (hydrogen bonding) between Co^{II} ions can influence the value of g_{eff}, and this can be resolved only if EPR measurements are carried out in both powder and solution samples.

The magnetic and EPR parameters of different high-spin Co^{II} complexes are shown in Table 3.[36] Based on the collective data and the aforementioned comments, several interesting conclusions can be drawn. First of all, it seems that for values of g_{eff} above 4.33 (in the EPR spectra of powder samples), the intermolecular interactions contribute significantly to the magnetic behavior of the system. In the case of $[Co(C_4H_8NO_3)_2(H_2O)_2]$,[36a] a weak exchange interaction transmitted through hydrogen bonds is proposed between neighboring Co^{II} centers in the exchange limit $0.25 < |J| < 1.2\ cm^{-1}$. To this end, the Brillouin function of an isolated $S = 1/2$ system could reproduce the magnetization curves, leading to the conclusion that its contribution is small. For all the other cases ($g_{eff} < 4.33$) no significant

Table 3. Magnetic and EPR properties of various Co^{II} carboxylate and mixed carboxylate-phosphonate compounds.

Compounds	g_{eff}[a] (EPR)	g_{eff} [b] (Magnetization)	Model $S = 3/2$[c]
This work	4.51(1) (p) 3.96(1) (s)	4.70(1) $zJ = -1.5\ cm^{-1}$	$g = 2.53(1)$, $D = 41(1)\ cm^{-1}$
$[Co(C_4H_8NO_3)_2(H_2O)_2]$[36a]	4.45(1) (p)	4.50(1)	$g = 2.60(1)$, $D = 114(4)\ cm^{-1}$
$[Co(C_2H_8O_6NP_2)_2(H_2O)_2]$[20]	4.10(1) (p) 4.10(1) (s)	4.20(1)	$g = 2.33$, $D = 40(1)\ cm^{-1}$ ($g_{\parallel} = 1.7$, $g_{\perp} = 2.53$), $D = 52(1)\ cm^{-1}$ $\lambda = 0.33$
$(NH_4)_4[Co(C_6H_5O_7)]_2$[21]	4.00(1) (p)	4.50(1)[d]	$g = 2.42$, $D = 0.83\ cm^{-1}$
$K_2[Co_2(C_6H_5O_7)_2(H_2O)_4]\cdot 6\ H_2O$[e][36b]	3.75(1) (s)	3.87(1)	–

[a] g_{eff} $[(g_x + g_y + g_z)/3]$ is derived from the EPR measurements performed in powder (p) or solution (s) samples. [b] g_{eff} is derived by simulation of the magnetization data at different temperatures using the Brillouin function for an isolated $S = 1/2$ system, or Equation (4) in the case of intermolecular interactions. [c] Fitting parameters (D, E, g) obtained from Equation (1) for the fit of the susceptibility data. [d] The simulation was carried out using the magnetization data from ref.[21]. [e] This complex is a dimer in the solid state. We only used the solution spectrum of the complex, since it dissociates into monomers in solution.[36b]

intermolecular interactions are observed. The significance of the aforementioned point is also exemplified in the small g_{eff} value of the frozen-solution spectrum, where the hydrogen-bonding system breaks apart and no longer exists. Secondly, the g_{eff} value derived from the magnetization data is not equal to the value obtained from EPR measurements due to the fact that, in the magnetization data, there is also some contribution from intermolecular interactions, a fact amply emphasized and alluded to in the magnetization study of this work.

Linking the Aqueous Chemistry of the Binary Co^{II}–H_5NTA2P System to the Organophosphonate Structural Features

In a simple and pH-specific manner, the employment of the binary system Co^{II}-(H_5NTA2P) led to the isolation of a clean product **1** in crystalline form. The idea was to initially explore the reactivity of the aforementioned system at low pH. The H_5NTA2P ligand projects important features that emerge due to its structure containing both carboxylic and phosphonic moieties (see below). Under such conditions, addition of ethanol contributed to the isolation of $[Co(C_4H_9O_8NP_2)(H_2O)_2]\cdot 2H_2O$ (**1**) at pH 1.5. The nature of **1** is that of a molecular type of lattice comprised of mononuclear units linked together through water molecules of crystallization and an extensive network of hydrogen bonds.

The carboxydiphosphonate ligand anchored onto the octahedral Co^{II} site reveals a coordination mode that reflects employment of all potential anchor sites in H_5NTA2P. Variable modes of phosphonate coordination have previously been observed in a plethora of metal organophosphonate complexes containing the phosphonate ligand termini in varying deprotonation states.[37] In the present case, the coordinated H_5NTA2P ligand loses two of its protons from the two terminal phosphonate groups, rendering each one of them singly deprotonated. As a result, the remaining carboxylic acid moiety remains protonated and, as such, it is anchored to the metal site. The double deprotonation of the H_5NTA2P ligand yields an overall charge of zero for the assembled mononuclear complex, affording the previously mentioned molecular type of lattice in **1**.

The nitrogen center plays a prominent role in the coordination of the H_5NTA2P ligand around Co^{II}. A strong interaction with the metal center brings it to a distance of 2.229(2) Å from Co^{II}. Thus, the tetradentate ligand imparts significant stability upon the resulting species. Due to the fact that the ligand itself employs four potential anchoring sites to bind the metal ion, the octahedral coordination environment is left with two unoccupied sites, which are occupied by water molecules from the reaction medium.

As a consequence of the molecular chemistry between the H_5NTA2P and Co^{II}, discrete moieties evolve as mixed carboxylate-phosphonate species in aqueous media. This is in contrast to the intermolecular chemistry previously observed between another diphosphonate ligand, namely iminodiphosphonic acid (IDA2P), and Co^{II}.[36b] There, the ligand promotes an intermolecular linkage of nearby Co^{II} centers, affording a molecular lattice with distinct structural features, at low pH.

The magnetic susceptibility and magnetization measurements on complex **1** support the presence of a high-spin octahedral Co^{II} species having a ground state with an effective spin of 1/2. EPR measurements in the solid state and in aqueous solution corroborate the magnetization data, suggesting the existence of a high-spin Co^{II} complex in solution. Such a complex would very likely include the ligand octahedral environment provided by H_3NTA2P^{2-} and the two water molecules.[37] To this end, both UV/Vis and EPR data suggest a species with a formulation not unlike that of the title complex $[Co(C_4H_9O_8NP_2)(H_2O)_2]^0$. A similar behavior has previously been observed for $[Co(C_2H_8O_6NP_2)_2(H_2O)_2]$.[20]

To the extent that the title complex is an aqueous species of Co^{II}, it appears that the aqueous distribution of species arising from the binary system Co^{II}–H_5NTA2P encompasses such components emerging at low pH. That, in turn, hints at the existence of other species that might participate in the requisite speciation at higher pH values. This contention is potentially exemplified by the nature of the H_5NTA2P ligand, with its mixed composition eliciting variable chemical coordination events around Co^{II} with equally variable protonation states. Furthermore, H_5NTA2P is a ligand that can be viewed as a derivative of the nitrilotriacetic acid ligand $(HOOCCH_2)_3N$ (H_3NTA), with the two terminal carboxylates replaced by phosphonates. Solution as well as synthetic studies have been carried out for dicarboxylic acids,[38,39] aminoalkylphosphonates, and IDA-derived phosphonate ligands, like *N*-(phosphonomethyl)glycine,[40] in the presence of various metal ions.[41,42] These studies suggest that these ligands bind metal ions like Co^{II} efficiently to form soluble complexes.[12a] Despite the fact that analogous studies with $(H_2O_3PCH_2)_2NCH_2COOH$ and Co^{II} have not been carried out, it would not be unreasonable to suggest that a similar chemistry may be unfolding in this system too. In this sense, solution investigations would be helpful in revealing the nature of the interaction as well as the properties of the arising species as a function of pH and molecular stoichiometry. Such studies are under way in our laboratory.

Given that solubility is a prerequisite for bioavailability of species eliciting interactions at the cellular level, the structural and molecular composition of complex **1** suggest that significant features of Co^{II} might be associated with interactions with biological targets. The distinct nature of H_5NTA2P allows both phosphorylated and carboxylic sidechains of abutting biomolecular sites to interact concurrently with Co^{II}, thus giving rise to soluble species. Even though studies of soluble bioavailable Co^{II}–carboxyphosphonate species have yet to be performed, they could provide significant insight into the nature and properties of binary or ternary Co^{II}–ligand species of potential biological value to variable activity pathways in human physiology. Along these lines, the value of $E_{1/2}$ (–0.40 V) observed in the cyclic voltammogram of **1** for Co^{II}/Co^{I} is an indicator

of the physicochemical properties bestowed on Co^{II} upon coordination by H_5NTA2P and tuned into in the biologically relevant redox potential range.

Potential Formation of Organophosphonate-Containing Materials

The nature and properties of organophosphonate substrates have drawn keen interest in the search for new materials containing a variety of metals. Numerous approaches and synthetic methodologies have been employed in the quest for metal-organophosphonate materials with varying structures. The search for new materials has targeted diverse applications, extending from electronics to catalysis. To that end, organophosphonic acid substrates like $H_2O_3PCH_2CH_2$-COOH, or diphosphonic acids[43] like $H_2O_3PRPO_3H_2$, have been employed with different R groups [C_6H_4, $(CH_2)_n$],[44] joining the phosphonate moieties, that influence the structural features of the derived material significantly (compare [$Co(C_4H_9O_8NP_2)(H_2O)_2$]·$2H_2O$ (**1**) with [$Zn_2\{O_2CCH_2NH$-$(CH_2PO_3)_2\}$]).[45,46] Such features include lattice parameters, shape, size, and dimensionality, all of which affect the applied chemistry in selective and specific low molecular mass (alcohol, amine, etc.) transformation processes.

One such key factor that influences the nature of the lattice formed in a solid-state material is hydrogen bonding. This dominates the lattice structure of **1** and involves the coordinated and solvent water molecules as well as the protonated phosphonate and carboxylate moieties. The extensive network of hydrogen bonds can be simplified if one attempts to assemble it step by step. Specifically, the mononuclear species of **1** are hydrogen bonded through O6–HO6···O1 (1 + *x*, *y*, *z*) and Ow1–Hw1B···O5 (–1 + *x*, *y*, *z*) interactions to form polymeric chains that extend in a direction parallel to the crystallographic *a* axis. These chains are further hydrogen bonded through an Ow2–Hw2B···O2 (*x*, *y*, –1 + *z*) interaction to form a two-dimensional network lying parallel to the crystallographic *ac* plane. As shown in Figure 2 (a), the layered structure thus formed contains vacancies between the mononuclear species. Furthermore, the involvement of the remaining protonated phosphonate and carboxylate moieties in hydrogen-bonding interactions [O3–HO3···O5 (1 – *x*, –0.5 + *y*, 1 – *z*) and O8–HO8···O4 (1 – *x*, –0.5 + *y*, –*z*)] leads to the extended 3D lattice structure of **1**. As shown in Figure 2 (b), tubular channels are formed down the crystallographic *a* axis, where the lattice water molecules are encapsulated. Ostensibly, hydrogen-bonding interactions between the encapsulated lattice water molecules and the protonated phosphonate and carboxylate groups of the ligand, as well as the coordinated water molecules, are responsible for the stabilization of the encapsulated solvent molecules.

The nature of the metal ion is another key factor in metal organophosphonate materials. To this end, phosphonate-containing pillared layered structures have been synthesized from vanadium, such as the material [(VO)(H_2O)-$\{O_3PCH_2NH(C_2H_4)_2NHCH_2PO_3\}$],[46,47a] while manganese- and cobalt-containing materials such as [$M\{O_3PCH_2NH(C_2H_4)_2NHCH_2PO_3\}$]·$H_2O$ (M = Mn^{II}, Co^{II}) have also been isolated.[47b] Numerous such materials have emerged in the past few years, with key representatives including the compounds [$Co\{(CH_3COO)_2NCH_2PO_3\}$-$(H_2O)_5$]·$H_2O$,[48] [$Co(C_2H_8O_6NP_2)_2(H_2O)_2$],[20] [$Co_2(O_3$-$PC_6H_4PO_3)(H_2O)_2$],[49] and [$Co_2(O_3PC_6H_4OC_6H_4PO_3)$]·$2H_2O$,[50] amongst others. Collectively, the physical and chemical properties of Co^{II}–organophosphonate materials signify the decisive role of features upon which rests the design of future compounds with specific attributes for potential selective applications. To this end, examination of the herein described binary Co^{II}-H_5NTA2P system under conditions far removed from a room-temperature environment (e.g. hydrothermal conditions) could, in principle, result in a material with distinct physical and chemical characteristics not necessarily similar to those observed in the title species **1**. This approach could prove to be effective in affording diverse species that could potentially participate in the aqueous binary speciation scheme and possess physicochemical characteristics associated with applications alluded to above in other cobalt-containing materials.

Conclusions

The mixed carboxydiphosphonate complex of Co^{II}, reflected in the structural formulation of [$Co(C_4H_9O_8NP_2)$-$(H_2O)_2$]^0 (**1**), contains basic structural features of species that might arise as a result of the interaction of Co^{II} with adjacent carboxy and phosphorylated sites on low molecular mass biotargets in biological fluids. Complex **1**, in fact, constitutes proof of a species arising from speciation of binary systems containing Co^{II} and simple phosphonate ligands.[40] In the absence of solution speciation studies on the specific Co^{II}-H_5NTA2P system, the synthetic efforts of this work prove the existence of discrete species with characteristic structural and chemical properties both in the solid state as well as in solution. Spectroscopic studies combined with cyclic voltammetric, magnetic, and EPR data in the solid state and in solution support the experimental observations and formulate the speciation signature of the investigated binary system, and hint at the existence of other, as yet elusive, species arising in a pH-dependent fashion across the pH physiological range under both room temperature and hydrothermal conditions. Albeit low, the pH at which the assembly of the investigated species was pursued gives clues to the physicochemical properties of soluble species that might become bioavailable in the presence of suitable molecular targets at the cellular level. The investigation of such interactions and in-depth research of related materials and their potential applications are currently being pursued in our laboratory.

Experimental Section

Materials and Methods: All experiments were carried out in the open air at room temperature. Nanopure-quality water was used

for all reactions. $Co(NO_3)_2 \cdot 6H_2O$ and *N*,*N*-bis(phosphonomethyl)-glycine (H_5NTA2P) were purchased from Aldrich.

Physical Measurements: FT-IR measurements were taken with a Perkin–Elmer 1760X FT-infrared spectrometer. UV/Vis spectra were recorded with a Hitachi U-2001 spectrophotometer in the range 200–1000 nm. The EPR spectra of complex **1** in the solid state and in aqueous solution were recorded with a Bruker ER 200D-SRC X-band spectrometer, equipped with an Oxford ESR 9 cryostat. The powder spectra were recorded at 9.4261 GHz in the temperature range 4–77 K. The solution spectra were recorded at 9.3979 GHz in the temperature range 4–23 K. Magnetic susceptibility data were collected on powdered samples of **1** with a Quantum Design SQUID susceptometer in the temperature range 2.3–300 K, under various applied magnetic fields. Magnetization measurements were carried out at three different temperatures in the field range 0–6 T. Fitting procedures for the acquired experimental data were applied through the use of Fortran programming routines relating to the Hamiltonians employed and the basic parameters *D*, *E*, and *g*.[20,21,36b] Elemental analyses were performed by Quantitative Technologies, Inc. Electrochemical measurements were carried out with a Uniscan Instruments Ltd. model PG580 potensiostat-galvanostat. The entire system was under computer control and supported by the appropriate computer software (Ui Chem. Version 1.08RD) running on Windows. The electrochemical cell used had platinum (disk) working and auxiliary (wire) electrodes; an Ag/AgCl electrode was used as reference electrode. The water used in the electrochemical measurements was of nanopure quality. KNO_3 was used as supporting electrolyte. Normal concentrations used were 1–6 mM in electroanalyte and 0.1 M in supporting electrolyte. Purified argon was used to purge the solutions prior to the electrochemical measurements.

Preparation of $[Co(C_4H_9O_8NP_2)(H_2O)_2]\cdot 2H_2O$ (1): $Co(NO_3)_2 \cdot 6H_2O$ (0.17 g, 0.58 mmol) and *N*,*N*-bis(phosphonomethyl)glycine (H_5NTA2P; 0.16 g, 0.59 mmol) were dissolved in nanopure water. The pH of the resulting solution was 1.5. This reaction mixture was stirred at room temperature for 10–15 min. Subsequently, the reaction flask was cooled to 4 °C in the presence of ethanol. A couple of weeks later pink prismatic crystals grew out of the solution. The crystalline material was collected by filtration, and was dried under vacuum. Yield: 0.14 g (≈ 61%). $C_4H_{17}CoNO_{12}P_2$ (392.06): calcd. C 12.24, H 4.34, N 3.57; found C 12.53, H 4.45, N 3.54.

X-ray Crystal Structure Determination of 1: X-ray quality crystals of compound **1** were grown from aqueous solution. A single crystal with dimensions $0.12 \times 0.40 \times 0.60$ mm^3 was mounted on a Crystal Logic dual-goniometer diffractometer equipped with a graphite-monochromated Mo-K_α radiation source. Unit-cell dimensions for **1** were determined and refined by using the angular settings of 25 automatically centered reflections in the range $11 < 2\theta < 23°$. Intensity data were measured by the θ–2θ scans technique. Throughout data collection, three standard reflections were monitored every 97 reflections, and showed less than 2% variation and no decay. Lorentz, polarization, and psi-scan absorption corrections were applied by using Crystal Logic software. Further experimental crystallographic details for **1**: $2\theta_{max} = 50°$; scan speed: 4.0° min^{-1}; scan range: $2.25 + \alpha_1\alpha_2$ separation; number of reflections collected/unique/used: 2670/2474 (R_{int} = 0.0198)/2474; 249 parameters refined; $F(000)$ = 402; $(\Delta/\sigma)_{max}$ = 0.015; $(\Delta\rho)_{max}/(\Delta\rho)_{min}$ = 0.341/–0.227 e Å^{-3}; GOF = 1.049; R/R_w (for all data), 0.0226/0.0611.

The structure of complex **1** (Table 4) was solved by direct methods using SHELXS-86,[51] and refined by full-matrix least-squares techniques on F^2 with SHELXL-97.[52] All non-H atoms in the structure of **1** were refined anisotropically. All H atoms in the structure of **1** were located by difference maps and were refined isotropically.

Table 4. Summary of crystal, intensity collection, and refinement data for $[Co(C_4H_9O_8NP_2)(H_2O)_2]\cdot 2H_2O$ (**1**).

Formula	$C_4H_{17}CoNO_{12}P_2$
Formula weight	392.06
Temperature [K]	298
Wavelength [Å]	0.71073, Mo-K_α
Space group	$P2_1$
a [Å]	7.566(3)
b [Å]	12.721(5)
c [Å]	7.361(3)
β [°]	96.271(13)
V [Å^3]	704.2(5)
Z	2
$D_{calcd.}/D_{measd}$ (Mg m^{-3})	1.849/1.83
Abs. coeff. (μ) [mm^{-1}]	1.504
Range of h,k,l	–8→8, –15→15, 0→8
Goodness-of-fit on F^2	1.049
w*	a = 0.0337 b = 0.1093
R[a]	R = 0.0226[b]
R_w[a]	R_w = 0.0610[b]

[a] R Values are based on F values, R_w values are based on F^2 $R = \frac{\sum \| F_o | - | F_c \|}{\sum (| F_o |)}$, $R_w = \sqrt{\sum [w(F_o^2 - F_c^2)^2] / \sum [w(F_o^2)^2]}$. [b] For 2468 reflections with $I > 2\sigma(I)$; $w^* = 1/[\sigma^2(F_o^2) + (aP)^2 + bP]$ where $P = [\mathrm{Max}(F_o^2,0) + 2F_c^2]/3$.

CCDC-283144 (for **1**) contains the supplementary crystallographic data for this paper. These data can be obtained free of charge from the Cambridge Crystallographic Data Center via www.ccdc.cam.ac.uk/data_request/cif.

Acknowledgments

This work was supported by a "Pythagoras" grant from the National Ministry of Education and Religious Affairs and by a "PENED" grant from the General Secretariat of Research and Technology, Greece. V.T. would like to thank Dr. I. Sanakis of the N.C.S.R "Demokritos", Athens, Greece, for the EPR measurements and Dr. C. Sangregorio of the Department of Chemistry, Florence, Italy, for magnetic data collection.

[1] T. D. M. Taylor, D. R. Williams, *Trace Element Medicine and Chelation Therapy*, Royal Society of Chemistry, Cambridge, **1995**.
[2] S. Balachandran, R. A. Vishwakarma, S. M. Monaghan, A. Prelle, N. P. J. Stamford, F. J. Leeper, A. R. Battersby, *J. Chem. Soc., Perkin Trans. 1* **1994**, 487–491.
[3] A. R. Battersby, *Acc. Chem. Res.* **1993**, *26*, 15–21.
[4] L. Debussche, M. Couder, D. Thibaut, B. Cameron, J. Crouzet, F. Blanche, *J. Bacteriol.* **1992**, *22*, 7445–7451.
[5] a) S. L. Roderick, B. W. Matthews, *Biochemistry* **1993**, *32*, 3907–3912; b) A. Ben-Bassat, K. Bauer, S.-Y. Chang, K. Myambo, A. Boosman, S. Chang, *J. Bacteriol.* **1987**, *169*, 751–757.
[6] M. S. Payne, S. Wu, R. D. Fallon, G. Tudor, B. Stieglitz, I. M. Turner Jr, M. J. Nelson, *Biochemistry* **1997**, *36*, 5447–5454.
[7] S. J. Lippard, J. M. Berg, *Principles of Bioinorganic Chemistry*, University Science Books, Mill Valley, CA (USA), **1994**, chapter 11, p. 336–347.
[8] E. M. N. Hamilton, S. A. S. Gropper, *The Biochemistry of Human Nutrition*, West Publishing Company, New York, **1987**, p. 298–301.

[9] H. M. Helis, P. de Meester, D. J. Hodgson, *J. Am. Chem. Soc.* **1976**, *99*, 3309–3312.

[10] G. L. Waldbott, *Health Effects of Environmental Pollutants*, C. V. Mosby, Co.: St. Louis, MO, USA, **1973**.

[11] a) T. Kiss, *Bioinorganic Chemistry* (Ed.: K. Burger), Ellis Horwood, Chichester, **1990**, p. 56; b) R. B. Martin, *J. Inorg. Biochem.* **1986**, *28*, 181–187; c) P. M. May, P. W. Linder, D. R. Williams, *J. Chem. Soc., Dalton Trans.* **1977**, 588–595; d) D. D. Perrin, *Nature* **1965**, *206*, 170.

[12] a) D. Sanna, I. Bodi, S. Bouhsina, G. Micera, T. Kiss, *J. Chem. Soc., Dalton Trans.* **1999**, 3275–3282; b) T. Kiss, *Bioinorganic Chemistry* (Ed.: K. Burger), Ellis Horwood, Chichester, **1990**, p. 56.

[13] a) J. Zubieta, *Comments Inorg. Chem.* **1994**, *16*, 153–183; b) C. Bhardwaj, H. Hu, A. Clearfield, *Inorg. Chem.* **1993**, *32*, 4294–4299; c) A. Clearfield, *Comments Inorg. Chem.* **1990**, *10*, 89–128.

[14] a) Q. Chen, J. Salta, J. Zubieta, *Inorg. Chem.* **1993**, *32*, 4485–4486; b) E. T. Clarke, P. R. Rudolph, A. E. Martell, A. Clearfield, *Inorg. Chim. Acta* **1989**, *164*, 59–63; c) P. R. Rudolph, E. T. Clarke, A. E. Martell, A. Clearfield, *J. Coord. Chem.* **1985**, *14*, 139–149.

[15] B. Bujoli, P. Palvadeau, J. Rouxel, *Chem. Mater.* **1990**, *2*, 582–589.

[16] a) Y. Zhang, A. Clearfield, *Inorg. Chem.* **1992**, *31*, 2821–2826; b) G. H. Huan, A. J. Jacobson, J. W. Johnson, E. W. Corcoran Jr, *Chem. Mater.* **1990**, *2*, 91–93; c) G. Cao, H. Lee, V. Lynch, T. E. Mallouk, *Inorg. Chem.* **1988**, *27*, 2781–2785.

[17] a) D. A. Burwell, K. G. Valentine, J. H. Timmermans, M. E. Thompson, *J. Am. Chem. Soc.* **1992**, *114*, 4144–4150; b) G. L. Rosenthal, J. Caruso, *Inorg. Chem.* **1992**, *31*, 3104–3106; c) M. B. Dines, P. C. Griffith, *Inorg. Chem.* **1983**, *22*, 567–569; d) M. B. Dines, P. M. DiGiacomo, *Inorg. Chem.* **1981**, *20*, 92–97.

[18] a) H. Byrd, J. K. Pike, D. R. Talham, *J. Am. Chem. Soc.* **1994**, *116*, 7903–7904; b) H. E. Katz, W. L. Wilson, G. Scheller, *J. Am. Chem. Soc.* **1994**, *116*, 6636–6640; c) S. B. Ungashe, W. L. Wilson, H. E. Katz, G. R. Scheller, T. M. Putrinski, *J. Am. Chem. Soc.* **1992**, *114*, 8717–8719; d) R.-C. Wang, Y. Zhang, H. Hu, R. R. Frausto, A. Clearfield, *Chem. Mater.* **1992**, *4*, 864–871; e) G. L. Rosenthal, J. Caruso, *Inorg. Chem.* **1992**, *31*, 144–145.

[19] a) G. Cao, T. E. Mallouk, *Inorg. Chem.* **1991**, *30*, 1434–1438; b) K. J. Frink, R.-C. Wang, J. L. Colon, A. Clearfield, *Inorg. Chem.* **1991**, *30*, 1438–1441.

[20] H. Jankovics, M. Daskalakis, C. P. Raptopoulou, A. Terzis, V. Tangoulis, J. Giapintzakis, T. Kiss, A. Salifoglou, *Inorg. Chem.* **2002**, *41*, 3366–3374.

[21] M. Matzapetakis, M. Dakanali, C. P. Raptopoulou, V. Tangoulis, A. Terzis, N. Moon, J. Giapintzakis, A. Salifoglou, *J. Biol. Inorg. Chem.* **2000**, *5*, 469–474.

[22] L. Kryger, S. E. Rasmussen, *Acta Chem. Scand.* **1972**, *26*, 2349–2359.

[23] T. Glowiak, W. Sawka-Dobrowolska, B. Jezowska-Trzebiatowska, *Inorg. Chim. Acta* **1980**, *45*, L105–L106.

[24] V. S. Sergienko, G. G. Aleksandrov, E. G. Afonin, *Zh. Neorg. Khim.* **1997**, *42*, 1291–1296.

[25] S. M. Godfrey, D. G. Kelly, C. A. McAuliffe, R. G. Pritchard, *J. Chem. Soc., Dalton Trans.* **1995**, 1095–1101.

[26] V. S. Sergienko, E. G. Afonin, G. G. Aleksandrov, *Zh. Neorg. Khim.* **1998**, *43*, 1002–1007.

[27] R. S. Drago, *Physical Methods in Chemistry*, W. B. Saunders Company, Philadelphia, **1977**, p. 359–410.

[28] A. B. P. Lever, *Inorganic Electronic Spectroscopy*, 2nd Edition, Elsevier, Amsterdam, **1984**, p. 480–490.

[29] a) B. N. Figgis, *Introduction to Ligand Fields*, Interscience Publishers, New York, **1966**; b) C. K. Jorgensen, *Adv. Chem. Phys.* **1963**, *5*, 33–146; c) C. J. Ballhausen, *Introduction to Ligand Field Theory*, McGraw-Hill Book Co.: New York, **1962**.

[30] a) C. Djordjevic, M. Lee, E. Sinn, *Inorg. Chem.* **1989**, *28*, 719–723; b) G. B. Deacon, R. Philips, *J. Coord. Chem. Rev.* **1980**, *33*, 227–250.

[31] a) D. E. C. Corbridge, *J. Appl. Chem.* **1956**, *6*, 456–465; b) R. C. Gore, *Discuss. Faraday Soc.* **1950**, *9*, 138–143; c) J. V. Bell, J. Heisler, H. Tannenbaum, J. Goldenson, *J. Am. Chem. Soc.* **1954**, *76*, 5185–5189; d) L. C. Thomas, R. A. Chittenden, *Spectrochim. Acta* **1964**, *20*, 467–487.

[32] a) R. A. McIvor, C. E. Hubley, *Can. J. Chem.* **1959**, *37*, 869–876; b) L. C. Thomas, R. A. Chittenden, *Chem. Ind. (London)* **1961**, 1913.

[33] a) D. S. Sagatys, C. Dahlgren, G. Smith, R. C. Bott, A. C. Willis, *Aust. J. Chem.* **2000**, *53*, 77–81; b) S. Shoval, S. Yariv, *Agrochimica* **1981**, *25*, 377–386; c) V. Subramanian, P. E. Hoggard, *J. Agric. Food Chem.* **1988**, *36*, 1326–1329.

[34] R. Boca, *Coord. Chem. Rev.* **2004**, *248*, 757–815.

[35] A. Abragam, B. Bleaney, *Electron Paramagnetic Resonance of Transition Ions*, Clarendon Press, Oxford, **1970**.

[36] a) A. C. Rizzi, C. D. Brondino, R. Calvo, R. Baggio, M. T. Garland, R. E. Rapp, *Inorg. Chem.* **2003**, *42*, 4409–4416; b) N. Kotsakis, C. P. Raptopoulou, V. Tangoulis, A. Terzis, J. Giapintzakis, T. Jakusch, T. Kiss, A. Salifoglou, *Inorg. Chem.* **2003**, *42*, 22–31.

[37] a) V. S. Sergienko, G. G. Aleksandrov, E. G. Afonin, *Kristallografiya* **2000**, *45*, 262–265; b) P. H. Smith, K. N. Raymomd, *Inorg. Chem.* **1988**, *27*, 1056–1061; c) T. Glowiak, W. Sawka-Dobrowolska, B. Jezowska-Trzebiatowska, A. Antonow, *J. Cryst. Mol. Struct.* **1980**, *10*, 1–10; d) P. Fenot, J. Darriet, C. Garrigou-Lagrange, *J. Mol. Struct.* **1978**, *43*, 49–60.

[38] a) S. P. Petrosyants, M. A. Malyarik, A. B. Ilyukhin, *Zh. Neorg. Khim.* **1995**, *40*, 769–775; b) B. B. Smith, D. T. Sawyer, *Inorg. Chem.* **1968**, *7*, 922–928.

[39] a) D. Mootz, H. Wunderlich, *Acta Crystallogr., Sect. B* **1980**, *36*, 445–447; b) N. J. Mammano, D. H. Templeton, A. Zalkin, *Acta Crystallogr., Sect. B* **1977**, *33*, 1251–1254; c) A. B. Corradi, C. G. Palmieri, M. Nardelli, M. A. Pellinghelli, M. E. V. Tani, *J. Chem. Soc., Dalton Trans.* **1973**, 655–658.

[40] a) R. J. Motekaitis, A. E. Martell, *J. Coord. Chem.* **1985**, *14*, 139–149; b) H. E. Lundager Madsen, H. H. Christensen, C. Gottlieb-Petersen, *Acta Chem. Scand. A* **1978**, *32*, 79–83.

[41] a) M. Wozniak, G. Nowogrocki, *Talanta* **1979**, *26*, 1135–1141; b) M. Wozniak, G. Nowogrocki, *Talanta* **1979**, *26*, 381–388; c) T. Kiss, G. Balla, G. Nagy, H. Kozlowski, J. Kowalik, *Inorg. Chim. Acta* **1987**, *138*, 25–30; d) B. Radomska, E. Matczak-Jon, W. Woiciechowski, *Inorg. Chim. Acta* **1986**, *124*, 83–85; e) T. I. Ignat'eva, A. N. Bovin, A. V. Yarkov, A. N. Chekhlov, E. N. Tsvetkov, O. A. Raevskii, *Koord. Khim.* **1989**, *15*, 1179–1185.

[42] a) T. Appleton, J. R. Hall, I. J. McMahon, *Inorg. Chem.* **1986**, *25*, 726–734; b) R. J. Motekaitis, I. Murase, A. E. Martell, *Inorg. Chem.* **1976**, *15*, 2303–2306.

[43] a) S. Drumel, P. Janvier, P. Barboux, M. Bujoli-Doeuff, B. Bujoli, *Inorg. Chem.* **1995**, *34*, 148–156; b) S. Drumel, P. Janvier, P. Barboux, M. Bujoli-Doeuff, B. Bujoli, *New J. Chem.* **1995**, *19*, 239–242.

[44] A. Choudhury, S. Natarajan, *Solid State Sci.* **2000**, *2*, 365–372.

[45] a) G. Cao, V. M. Lynch, J. S. Swinnea, T. E. Mallouk, *Inorg. Chem.* **1990**, *29*, 2112–2117; b) G. B. Hix, V. J. Carter, D. S. Wragg, R. E. Morris, P. A. Wright, *J. Mater. Chem.* **1999**, *9*, 179–185.

[46] a) J.-G. Mao, Z. Wang, A. Clearfield, *N. J. Chem.* **2002**, *26*, 1010–1014; b) V. Soghomonian, Q. Chen, R. C. Haushalter, J. Zubieta, *Angew. Chem. Int. Ed. Engl.* **1995**, *34*, 223–226.

[47] a) V. Soghomonian, R. Diaz, R. C. Haushalter, C. J. O'Connor, J. Zubieta, *Inorg. Chem.* **1995**, *34*, 4460–4466; b) R. LaDuca, D. Rose, J. R. D. DeBord, R. C. Haushalter, C. J. O'Connor, J. Zubieta, *J. Solid State Chem.* **1996**, *123*, 408–412.

[48] J.-G. Mao, A. Clearfield, *Inorg. Chem.* **2002**, *41*, 2319–2324.

[49] D.-K. Cao, S. Gao, L.-M. Zheng, *J. Solid State Chem.* **2004**, *177*, 2311–2315.

[50] M. M. Gomez-Alcantara, A. Cabeza, M. Martinez-Lara, M. A. G. Aranda, R. Suau, N. Bhuvanesh, A. Clearfield, *Inorg. Chem.* **2004**, *43*, 5283–5293.
[51] G. M. Sheldrick, *SHELXS-86: Structure Solving Program*, University of Göttingen, Germany, **1986**.
[52] G. M. Sheldrick, *SHELXL-97: Structure Refinement Program*, University of Göttingen, Germany, **1997**.
Received: September 19, 2005
Published Online: March 30, 2006

